Geophysical Research Letters

RESEARCH LETTER
10.1029/2022GL100715

Tropical Pacific and North Atlantic Sea Surface Temperature Patterns Modulate Mississippi Basin Hydroclimate Extremes Over the Last Millennium

Xinyue Luo[1], Sylvia Dee[1], Trinity Lavenhouse[2], Samuel Muñoz[3,4], and Nathan Steiger[5,6]

[1]Department of Earth, Environmental, and Planetary Sciences, Rice University, Houston, TX, USA, [2]Department of Physics and Astronomy, George Mason University, Fairfax, VA, USA, [3]Department of Marine and Environmental Sciences, Marine Science Center, Northeastern University, Nahant, MA, USA, [4]Department of Civil and Environmental Engineering, Northeastern University, Boston, MA, USA, [5]Institute of Earth Sciences, Hebrew University of Jerusalem, Jerusalem, Israel, [6]Lamont-Doherty Earth Observatory, Columbia University, Palisades, NY, USA

Key Points:

- We investigate the drivers of Mississippi River basin hydroclimate extremes over the last millennium
- Paleoclimate data assimilation reveals dry (wet) conditions during central Pacific (eastern Pacific) El Niño events
- Self-organizing maps expose a North Atlantic tripole pattern which modulates moisture supply over the Ohio river basin

Supporting Information:

Supporting Information may be found in the online version of this article.

Correspondence to:

X. Luo,
xl91@rice.edu

Citation:

Luo, X., Dee, S., Lavenhouse, T., Muñoz, S., & Steiger, N. (2023). Tropical Pacific and North Atlantic sea surface temperature patterns modulate Mississippi basin hydroclimate extremes over the Last Millennium. *Geophysical Research Letters*, *50*, e2022GL100715. https://doi.org/10.1029/2022GL100715

Received 3 AUG 2022
Accepted 17 DEC 2022

Abstract Mississippi River basin floods impart large socioeconomic impacts over the central United States. Improving flood predictability depends on our understanding of the dynamical controls on Mississippi basin hydroclimate. However, short instrumental records make it difficult to constrain the connections between flooding and climate variability. Here, we use the Paleo Hydrodynamics Data Assimilation product, spanning the Last Millennium, to investigate the impacts of tropical Pacific and North Atlantic sea surface temperature (SST) variability on hydrological extremes across the Mississippi River and its major tributaries. Wet extremes are associated with strong El Niño-like warming over the tropical Pacific, but specific SST patterns matter: dry (wet) conditions occur during Central Pacific (Eastern Pacific) El Niño events. The influence of North Atlantic SSTs is less clear, but cool SSTs contribute to Ohio basin wet extremes. These results are relevant for seasonal-to-interannual flood hazard prediction on the fourth largest river basin in the world.

Plain Language Summary Large floods on the Mississippi River during the last century have proven costly, both in economic and social terms. To improve flood hazard prediction, it is critical to understand how patterns in Earth's climate system contribute to Mississippi floods. However, relatively few flooding events occurred during the 20th century, which limits our ability to evaluate the statistics of these events. This work seeks to use records of past climate (from archives such as corals, ice cores, and trees) spanning the last 1,000 years to investigate the drivers of Mississippi flooding. Specifically, we focus on how sea surface temperature (SST) changes over the tropical Pacific and North Atlantic affect the hydrological cycle over the basin. We find that very wet periods are strongly associated with warm SSTs in the eastern tropical Pacific, but central tropical Pacific warming causes dry conditions. The impact of North Atlantic SST variability is much weaker, but, in combination with tropical Pacific warming, cool SSTs over the North Atlantic can amplify wet conditions over the eastern Mississippi River basin's tributaries. Our results harbor implications for seasonal-to-interannual flood hazard prediction, and can help stakeholders prepare for and mitigate flooding in the 21st century.

1. Introduction

The Mississippi River system spans the central United States and plays a major role in the regional economy through its relationship with transportation, agriculture, and urban centers (Figure 1a). Significant efforts have been made throughout the 20th century to monitor, predict, and manage discharge and flooding in the Mississippi River basin (Allison et al., 2012; L. M. Smith & Winkley, 1996). However, large floods on the Mississippi River continue to cause significant damage both in economic and social terms, destroying infrastructure, disrupting trade, and displacing millions of people (Alfortish et al., 2012; Barry, 2007).

Modes of natural climate variability, such as the El Niño-Southern Oscillation (ENSO) and the Atlantic Multi-Decadal Oscillation (AMO), affect Mississippi River hydroclimate and could inform seasonal to decadal flood forecasting (Enfield et al., 2001; Mallakpour & Villarini, 2016; Muñoz & Dee, 2017; Rogers & Coleman, 2003; Tootle et al., 2005; Twine et al., 2005). For example, increased precipitation during El Niño events influences the hydrological cycle and increases flood risk over the Mississippi River basin via a seasonal response of soil moisture storage, runoff, and river discharge (J. Chen & Kumar, 2002; Dai et al., 2009; Tootle

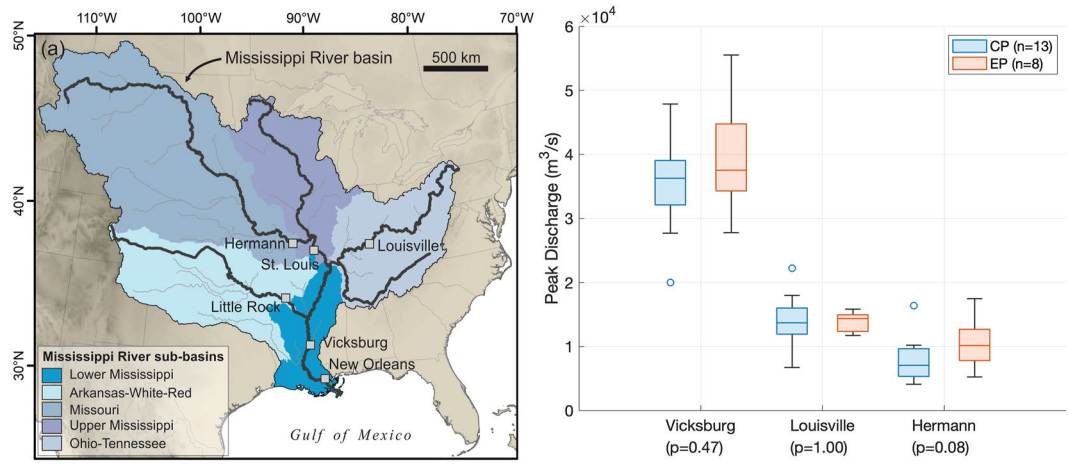

Figure 1. Mississippi River system and non-robust instrumental stream gauge statistics on El Niño-Southern Oscillation variability: (a) Mississippi River basin and major sub-basins (Missouri, Ohio, Arkansas-White Rivers, and Lower Mississippi mentioned in text); (b) boxplots of peak annual discharge (m^3/s) during Central Pacific (CP) and Eastern Pacific (EP) El Niño events (defined in Yu and Zou (2013)) at river gauges: Vicksburg (lower Mississippi), Louisville (lower Ohio), and Hermann (lower Missouri). *P*-values of Wilcoxon rank-sum test on the differences between discharges during CP and EP El Niño events are shown in (b).

et al., 2005; Twine et al., 2005). In addition, recent studies have suggested that two types of El Niño events, classified as eastern Pacific (EP) El Niño and central Pacific (CP) El Niño based on their sea surface temperature anomaly (SSTA) patterns (Ashok et al., 2007; Kao & Yu, 2009; Kug et al., 2009; Luo et al., 2022; Takahashi et al., 2011), have distinct impacts on Mississippi basin hydroclimate: CP El Niño events lead to decreased precipitation and soil moisture storage over the Ohio–Mississippi Valley compared to EP El Niño events (Liang et al., 2014; Ning & Bradley, 2015; Yu & Zou, 2013).

Beyond ENSO, North Atlantic SST variability also affects soil moisture and runoff within the Mississippi River basin by modulating the strength and position of the North Atlantic Subtropical High (NASH) (Enfield et al., 2001; Hu et al., 2011; J. A. Smith & Baeck, 2015; Tootle et al., 2005). For example, during AMO cold phases, cold SST anomalies generate anti-cyclonic flows, strengthening the NASH and shifting its center toward the west (Enfield et al., 2001; Hu et al., 2011). This in turn yields an increase in precipitation frontal flows which enhances flood risk over the Mississippi River compared to AMO warm phases (Enfield et al., 2001; Feng et al., 2011; Hu et al., 2011; Mallakpour & Villarini, 2016; McCabe & Wolock, 2014; Rogers & Coleman, 2003). North Atlantic Tripole (NAT) SST patterns also interact with the North Atlantic Oscillation (NAO) to alter moisture supply over the central U.S. over interannual-to-decadal time scales (S. Chen et al., 2020; Durkee et al., 2008; Peng et al., 2003; Sutton et al., 2000; Z. Wu et al., 2009).

Given the observed hydrologic impacts of ENSO and the North Atlantic SSTs on the Mississippi River, it is possible that flood forecasting across the basin over seasonal to decadal time-scales could be improved by constraining the connections between flood hazard and predictable modes of climate variability (Kiem et al., 2003; Stedinger & Griffis, 2011). However, the limited number of extreme floods that occurred during the instrumental period make it difficult to quantify and evaluate the dynamical controls on hydroclimate extremes over the Mississippi River basin with robust statistics. Instrumental flood gauge measurements indicate that EP El Niño events generate more river discharge compared to CP El Niño events; however, the significance of this difference varies for different tributaries (Figure 1b). The underlying dynamics are also difficult to constrain using 20th century data alone; previous studies have only investigated a handful of CP and EP El Niño events, on the order of ∼10 each (Liang et al., 2014; Ning & Bradley, 2015).

To address these shortcomings, highly-resolved paleoclimate data assimilation (DA) products spanning the Last Millennium (LM), such as the Paleo Hydrodynamics Data Assimilation product (PHYDA, Steiger et al., 2018), are used in this study to augment 20th century instrumental data. PHYDA takes advantage of multi-proxy archives and model physics, complementing prior work using LM climate model simulations to investigate ENSO and Mississippi flood hazard (Muñoz & Dee, 2017). While proxy coverage over the North American continent is

robust due to tree ring availability, individual proxy record coverage (mostly from corals) is somewhat sparse over the central/eastern tropical Pacific (Steiger et al., 2018; PAGES2k Consortium, 2017) (see Figure S1 in Supporting Information S1). Paleoclimate DA fills in the data gaps in a dynamically-consistent framework, facilitating investigation of spatially-complete SST patterns over hundreds of years. Here, we focus on the contributions of North Atlantic SST variability and ENSO SST pattern to hydroclimate extremes of the Mississippi River and its major tributaries (Missouri, Ohio, Arkansas-White Rivers, and Lower Mississippi; Figure 1a). Specifically, we aim to answer two key questions: (a) What are the primary modes of SST patterns, including ENSO flavors, over the tropical Pacific that contribute to hydroclimate extremes over the Mississippi River basin and its major tributaries during the LM? (b) How does North Atlantic SST variability affect hydroclimate conditions over the Mississippi basin and its major tributaries during the LM?

2. Data and Methods

2.1. The Paleo Hydrodynamics Data Assimilation Product

The Paleo Hydrodynamics Data Assimilation Product (PHYDA) is a hydroclimate-focused paleoclimate DA product that reconstructs global temperature, hydroclimate, and dynamical variables over the past 2,000 years (Steiger et al., 2018). PHYDA employs an offline ensemble Kalman filter approach (Oke et al., 2002), which combines 2,978 proxy time series spanning different periods of the Common Era (see Figure 1 in Steiger et al., 2018) with a bias-corrected version of the Community Earth System Model Last Millennium Ensemble (CESM LME, Otto-Bliesner et al. (2016)). The temporal and spatial coverage afforded by PHYDA over the tropical Pacific and North America is given in Figure S1 in Supporting Information S1. PHYDA reconstructs climate variables at an annual mean resolution based on a hydrological year (April to March of next year, e.g., April 1997–March1998), boreal summer mean (June through August; JJA), and austral summer mean (December through February; DJF). We employ the ensemble mean of the AMO index to represent AMO variability, DJF mean and annual mean two-meter (2 m) air temperature as an approximation for SST (e.g., Cayan, 1980), and annual mean Palmer Drought Severity Index (PDSI, Palmer, 1965) to evaluate Mississippi River hydroclimate extremes over the LM.

PHYDA has been thoroughly validated in previous publications, which show that PHYDA reconstructs a more realistic AMO index, ENSO SST temporal variability, and ENSO spatial patterns compared to its model prior, CESM (Luo et al., 2022; Steiger et al., 2018, 2019). Given its large bearing on this work, we also here independently validate the PDSI time series over the Mississippi River basin using two instrumental PDSI data products constructed by Sheffield et al. (2006, 2012) and Dai et al. (2004). The results show that PHYDA exhibits strong agreement with observed multi-decadal Mississippi PDSI variability over the 20th century (Figure S2 in Supporting Information S1), with an annual correlation coefficient of 0.8.

We note that we focus on PHYDA instead of other available DA reconstructions (e.g., the Last Millennium Reanalysis, Hakim et al., 2016; Tardif et al., 2019) due to PHYDA's emphasis on reconstructing global hydroclimate as opposed to temperature; the inclusion of hundreds of additional hydroclimate-sensitive proxy records has been shown to improve the reconstruction skill for ENSO-related climate patterns as well (Steiger et al., 2018). These and other factors (e.g., the use of a hydrological year) make PHYDA the best choice for this analysis.

2.2. Climate Index Definitions

The reconstructions from PHYDA yield both mean state and variance changes going back in time; like all other DA-based reconstructions, PHYDA's time series variance reduces further back in time as proxy information decreases. To avoid the possibly confounding influences of both mean state changes and the variance reductions on our extremes analysis, we have removed the running 30-year mean of the PDSI and SST time series to compute anomalies. To define wet extremes, we have normalized the basin-mean PDSI anomalies by the 30-year running standard deviation. Extreme wet events are then defined as the top 1% and 10% of the normalized PDSI anomaly time series over the LM; normal years are defined as normalized PDSI anomalies within the interquartile range (IQR, 25%–75%).

We use the Niño 3.4 index (SSTAs averaged across the region of 5°S–5°N, 170°W–120°W) to characterize ENSO variability. In addition, CP and EP El Niño events are defined based on the C and E index method

(Takahashi et al., 2011), which has been validated for PHYDA in previous work (Luo et al., 2022). C and E indices are computed based on Empirical Orthogonal Function (EOF) analysis on tropical Pacific (30°S–30°N, 120°E–80°W) SSTAs following the removal of the running 30-year mean, as mentioned above. The first two principal components (PCs) of the EOF analysis are projected onto a 45°-rotated orthogonal coordinate axis ($C = (PC1 + PC2)/\sqrt{2}, E = (PC1 - PC2)/\sqrt{2}$) to generate the C and E indices, respectively. CP El Niño events are defined when the C index exceeds 1σ *and* the value of the E index for CP definition years. Similarly, EP El Niño events are defined for those years where the E index exceeds 1σ *and* exceeds the C index. ENSO teleconnections are defined as PDSI anomalies normalized by the 30-year running standard deviation of the Niño 3.4 index to remove the impact of ENSO amplitude (S. Dee et al., 2020; Stevenson, 2012), and to account for the impacts of decreasing proxy availability back in time (S. G. Dee & Steiger, 2022; Steiger et al., 2018). Patterns of CP and EP El Niño and hydroclimate teleconnections are generated as the composite averages of SSTA and PDSI anomalies. For comparisons between hydroclimate conditions associated with CP and EP El Niño events, the probability density functions (PDFs) of PDSI anomalies are computed.

The SST-based AMO index is used to characterize AMO variations and define its warm and cold phases. PHYDA reconstructs a North Atlantic SST index (SST averaged over 0°N–65°N, 0°W–80°W), which is a non-detrended and non-smoothed version of the AMO (Steiger et al., 2018). We applied a 20-to-100-year Butterworth bandpass filter to the original North Atlantic SST index to isolate AMO signals from long-term mean-state changes. The AMO index is then defined here as the filtered time series. Given the variance reduction in the PHYDA reconstruction back in time (Steiger et al., 2018), the AMO index is first normalized with the 100-year moving standard deviations. AMO warm phase years are chosen if normalized AMO indices exceed +1 standard deviations from the mean ($+1\sigma$). Conversely, AMO cold phases are defined lower than -1σ.

2.3. Self-Organizing Map and Frequency Analysis

Self-organizing map (SOM) analysis is employed to isolate the tropical Pacific SSTA patterns associated with extreme hydroclimate conditions. SOM is an unsupervised machine learning approach that projects high-dimensional data information onto two-dimensional space while preserving the data structure, and classifies each input through finding the best-matching mode based on minimizing Euclidean distance (Kohonen, 1990; Liu & Weisberg, 2011). The DJF mean SSTA fields over the LM in PHYDA are assigned by the SOM algorithm to the spatial SSTA patterns of a pre-set number of clusters, or "nodes" (6 nodes are analyzed in the main text, with additional choices shown in the Supplement) to represent different tropical Pacific/North Atlantic SST modes. The resulting SSTA patterns associated with each cluster represent the composites of events with maximum similarity in their SSTA fields (Johnson et al., 2008), thus the SOM nodes directly represent the underlying physical patterns (Johnson, 2013; Liu et al., 2006). The SST fields are detrended by removing the 100-year smoothing of individual grid point time series (Horton et al., 2015), and are area-weighted according to the cosine of latitude prior to SOM computation. Then, a frequency-based analysis of each SSTA pattern accompanying extreme hydroclimate events is conducted to estimate the frequency change associated with each node in extreme wet years compared to normal years. We also conduct a 1,000-iteration bootstrap resampling drawn from the normal years (IQR) to check whether the frequency changes observed during extreme wet years indicate a departure from randomness. As a complement to the information afforded by composite averaging patterns, SOM and frequency analyses provide information surrounding the temporal evolution of the SSTA field in the years during hydroclimate extremes (S. G. Dee & Steiger, 2022; Steiger et al., 2019).

3. Results

3.1. Tropical Pacific SSTA Modes and Wet Extremes Over Mississippi River Basin

We first use a SOM algorithm (Section 2.3) to extract the top 6 SOM nodes of tropical Pacific SSTA patterns over the past 2,000 years in PHYDA (Figures 2a–2f). The percentage numbers at the top of each map panel show the frequency changes for different SSTA patterns in wet extreme events (top 10%) relative to the frequency of those same patterns in normal years (IQR). All El Niño-like SSTA patterns (SOMs 1, 2, and 4) show increases in frequency for extreme wet conditions over the Mississippi River basin, while all La Niña-like SSTA patterns (SOMs 3, 5, and 6) show decreases in frequency. Figure 2g shows that only the shift in SOM2 (+107%), which is characterized by a strong El Niño-like mean SSTA pattern (Figure 2b), exceeds the null distribution generated

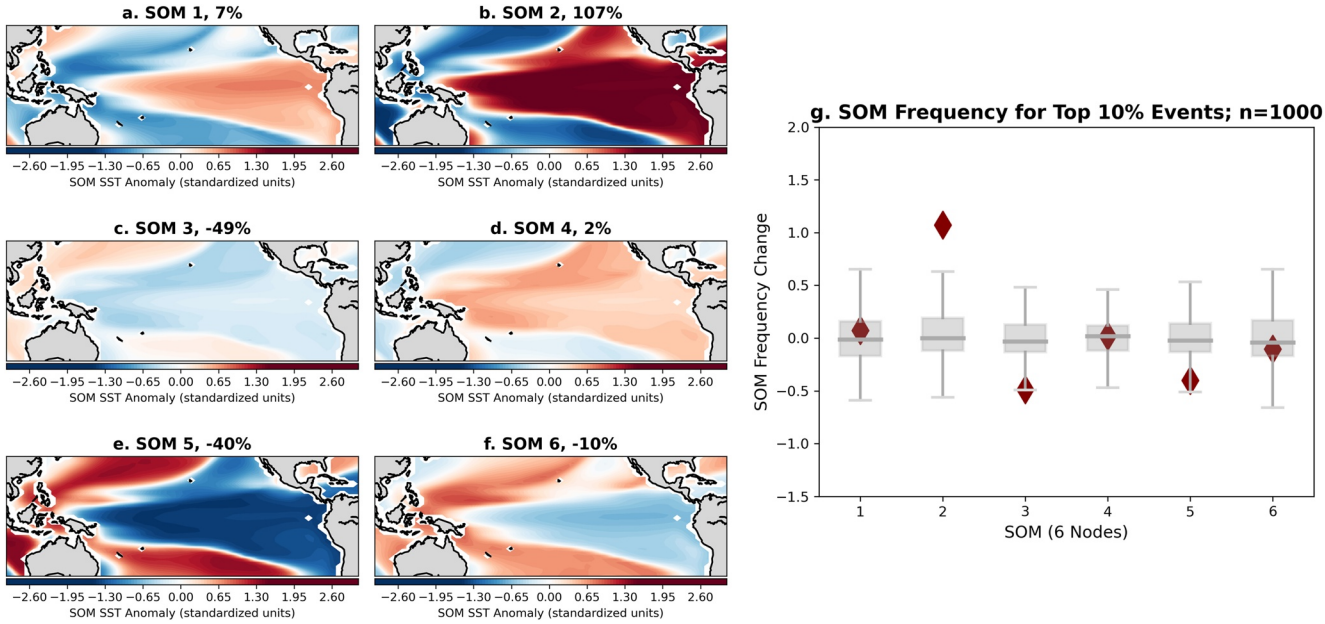

Figure 2. Self-organizing map and frequency analysis for the top 10% wet extreme events over the Mississippi River basin: (a–f) Show the tropical Pacific sea surface temperature anomaly patterns (in standardized units) associated with six nodes in the self-organizing map (SOM) computation. Each SOM node is labeled with the percent change in frequency for wet extreme events. (g) Shows the frequency analysis for each SOM node. Frequency changes during wet extreme events are shown as red diamonds; 1,000 iterations of a resampling test of background/normal event frequency changes are shown as gray box plots.

by resampling from the normal-year node frequency changes. This result suggests that when wet extreme events occur over the Mississippi River basin, they are accompanied by a substantial increase in the frequency of strong El Niño-like warming patterns over tropical Pacific. Thus, extreme wet conditions over the Mississippi River basin are more strongly associated with strong El Niño-like SSTA patterns compared to other SSTA patterns over tropical Pacific. We conducted the same analysis on the top 1% of extreme wet events (Figure S3 in Supporting Information S1) with all SOM SSTA patterns (as in Figures 2a–2f). The frequency changes of each SSTA pattern for the top 1% events show that SOM 1 and 2 (characterized by weaker and stronger El Niño-like SSTA patterns, respectively) show frequency increases during top 1% extreme hydroclimate conditions over the LM. The frequency increases for both SOM 1 and 2 are unusual compared to the background range (Figure S3 in Supporting Information S1). In general, these results suggest strong El Niño-like SSTA patterns occur more frequently over the tropical Pacific during wet extreme conditions over Mississippi River basin.

To check the sensitivity of our results to the number of SOM nodes, we recomputed frequency changes using 4 and 8 SOM nodes for both the top 1% and 10% wet extreme years (Figures S4–S7 in Supporting Information S1). Consistent with the results using 6 SOM nodes, the strong El Niño-like warming patterns over the tropical Pacific (SOM 2 for both 4 and 8 SOM maps) show large frequency increases, exceeding the null distribution (Figure S5–S7 in Supporting Information S1). An exception is the 4-node SOM analysis for the top 1% extreme events (frequency increases in Figure S4 in Supporting Information S1, but the change is within the null distribution). Taken together, the frequency increase for strong El Niño-like SSTA patterns is robust, even considering different SOM node numbers and wet extreme definitions. Wet extreme conditions over the Mississippi River basin are associated with strong El Niño-like mean-state warming over the tropical Pacific during the LM.

Finally, to further evaluate the drivers of wet extreme conditions over the different tributary sub-basins (Missouri, Ohio, Arkansas, and Lower Mississippi; Figure 1a) of the Mississippi River, we conducted the same frequency analyses of the SOM SSTA patterns associated with wet extreme events (top 1% or 10%) over each tributary (Table S1 in Supporting Information S1). Noting that the SOM SSTA patterns are still held constant (as in Figures 2a–2f), the frequency of SOM 2 (strong El Niño-like warming, Figure 2b) increases by 200% for the top 1% events and 155% for the top 10% events over the Missouri basin, and increases by 88% for the top 10% events over the Arkansas basin (Table S1 in Supporting Information S1), changes which all exceed the "normal-years" frequency distribution in each sub-basin. In contrast, the frequency changes associated with wet extremes over

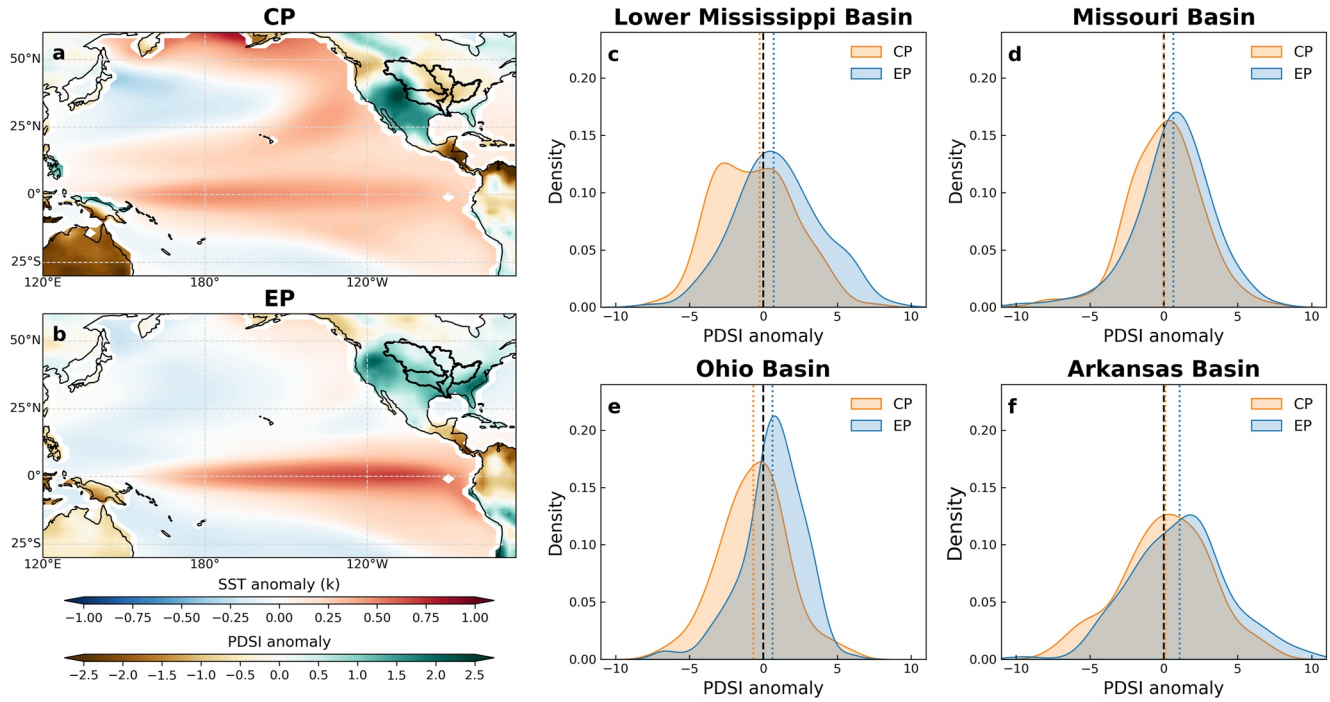

Figure 3. Central Pacific (CP) and Eastern Pacific (EP) El Niño and associated hydroclimate conditions over the Mississippi River basin and its tributaries: sea surface temperature anomaly and Palmer Drought Severity Index (PDSI) anomaly map composites from the Paleo Hydrodynamics Data Assimilation product for (a) CP and (b) EP El Niño events. The Mississippi River basin and its major tributaries (Missouri, Ohio, Arkansas, and Lower Mississippi) are outlined with black lines. (c–f) Show the probability density functions of mean PDSI anomalies over Lower Mississippi, Missouri, Ohio, and Arkansas basin, respectively, during CP (orange) and EP (blue) El Niño events. The distributions are significantly different between CP and EP El Niño events with $p < 0.005$ in a Wilcoxon rank-sum test. Dotted lines represent the average of each distribution. All black dashed lines represent 0 PDSI anomaly. Here, PDSI anomalies are normalized by the 30-year running standard deviation of the Niño 3.4 index.

the Ohio and Lower Mississippi basins do not shift beyond the "normal-year" frequencies for any SOM SSTA patterns (Table S1 in Supporting Information S1). The unusual frequency increases of SOM 2 for Missouri and Arkansas rivers suggest that extreme hydroclimate responses to strong El Niño-like warming are spatially heterogeneous over the Mississippi River basin; increased moisture supply over the Missouri and Arkansas basins, the western tributaries of the Mississippi, provide the major contributions to basin-wide wet extreme conditions associated with strong El Niño-like SSTA patterns in the tropical Pacific.

3.2. Mississippi River Basin Hydroclimate Associated With CP and EP El Niño

To extend our analysis of El Niño SSTA pattern impacts on Mississippi hydroclimate, the definition methods described in Section 2.2 were applied to extract CP and EP El Niño events. The composites and PDFs of CP and EP El Niño event PDSI anomalies over the basin show how the hydroclimate patterns respond to distinct El Niño SSTA patterns throughout the LM (Figure 3). In general, the entire Mississippi River basin exhibits lower PDSI during CP El Niño events (dry conditions), but increased PDSI during EP El Niño events (wet conditions, Figures 3a and 3b). In particular, dry conditions are more intense over the Ohio and Lower Mississippi basins during CP El Niño events (Figure 3a). In contrast, dry conditions in the Missouri and Arkansas basins are distributed mainly in the eastern part of each basin, while wet conditions are distributed mainly around the western boundary of each basin (Figure 3a). During EP El Niño events, wet conditions over the Arkansas basin are more intense compared to other sub-basins (Figure 3b). The PDFs for the sub-basins show that PDSI during EP El Niño events shifts significantly ($p < 0.005$ in Wilcoxon rank-sum test, given the non-normal distribution of basin hydroclimate in Figure 3) toward positive PDSI anomalies (wet conditions) for all major tributaries (Figures 3c–3f), consistent with the mean hydroclimate patterns shown in Figure 3b. PDFs associated with CP El Niño events generally exhibit decreased PDSI compared to EP El Niño events for all sub-basins. However, the magnitudes of changes in PDSI are spatially heterogeneous. The Ohio basin shows the largest decrease in its

PDSI PDF compared to other basins (Figure 3e), consistent with the more intense dry conditions during CP El Niño shown in Figure 3a. The Missouri and Arkansas basins show a less pronounced decrease in PDSI PDFs, with mean hydroclimate conditions around 0 during CP El Niño events (Figures 3d and 3f), consistent with the mapped PDSI patterns in Figure 3a. Taken together, most of the Mississippi River basin experiences wet conditions during EP El Niño events but dry conditions during CP El Niño events on average during the LM. For the major tributaries, the hydroclimate conditions are spatially heterogeneous; the differences between two El Niño types are most prominent over the Ohio basin.

3.3. North Atlantic SST Variability and Mississippi River Basin Hydroclimate

The AMO's impacts on precipitation and river flows over the U.S. during the instrumental era have been evaluated in previous work (Enfield et al., 2001; Hu et al., 2011; Rogers & Coleman, 2003). To further investigate the connection between Mississippi wet extremes and AMO-related SST variability during the LM, PDFs of AMO indices during wet extreme events (top 1% and 10%) over Mississippi tributaries (Lower Mississippi, Missouri, Ohio, and Arkansas) are computed and compared to IQR "normal" years (Figures 4a–4h). The results show that PDFs of AMO indices during wet extreme events versus normal years are not significantly different (in a Wilcoxon rank-sum test) (Figures 4a–4h), except for the top 1% wet events over Ohio basin, wherein the AMO index shifts toward its warm phase (positive AMO index, Figure 4e). The results indicating that the averaged AMO indices are close to 0 (neutral phase) during wet extreme events for all major tributaries except for the Ohio suggests that, on average, the AMO's impact over most of Mississippi River basin during the LM is small. Composites of SSTA and PDSI anomalies for both phases of the AMO (as defined in Section 2.2) show dry conditions over basins, except for the Lower Mississippi, which shows slightly wetter conditions during AMO warm phases (Figure S8 in Supporting Information S1). The magnitude of drying during both AMO phases is sensitive to the phase definition (i.e., using 1, 1.5, or 2σ departures), as shown in Figures S8–S10 in Supporting Information S1. This result contrasts with previous work evaluating instrumental records and paleo-records, which suggest that precipitation and streamflow increase over the Mississippi basin during cold phases of the AMO (Enfield et al., 2001; Hu et al., 2011; Muñoz et al., 2018; Rogers & Coleman, 2003).

To evaluate Atlantic impacts beyond the AMO, we investigated the average North Atlantic SST patterns associated with wet extremes over the Mississippi River basin. Composites of SSTA over the North Atlantic during wet extreme events consistently show cooling over the extratropical western North Atlantic (Figures 4i–4p). SOM analysis shows that Mississippi wet extremes are significantly associated with a warm-cold-warm (WCW) tripole pattern of NAT SSTs (SOM5 in Figure S11 in Supporting Information S1). By tributary, for the Lower Mississippi basin, the top 1%–10% wettest years are associated with mean cooling over the North Atlantic (Figures 4i and 4j). However, our SOM analysis yields no significant connection between North Atlantic SST patterns and Lower Mississippi wet extremes (Table S2 in Supporting Information S1). For the Ohio River basin, the top 1% wet events are associated with WCW tripole SST patterns accompanied by EP El Niño-like patterns (Figure 4m and Figure S10e in Supporting Information S1), while the top 10% wet events show a general cooling pattern (Figure 4n). In SOM and frequency analyses, Ohio wet extremes show significant association with the WCW tripole pattern (SOM5 in Figure S11 and Table S2 in Supporting Information S1). For the Missouri and Arkansas basin, the top 1% and 10% wet extremes are generally associated with WCW tripole patterns (Figures 4k and 4l), but are also accompanied by strong El Niño-like patterns (Figures S12c and S12d in Supporting Information S1). SOM analyses show that wet extremes over the Missouri and Arkansas basin are significantly connected with a strong WCW tripole pattern (with strong tropical North Atlantic warming, SOM6 in Figure S11 and Table S2 in Supporting Information S1).

Evidence surrounding the tropical Pacific impacts on Ohio wet extremes is conflicting: SOM analysis suggests Ohio wet extremes do not respond substantially to any tropical Pacific SSTA patterns (Table S1 in Supporting Information S1); meanwhile, Figure 3 indicates the Ohio basin is highly sensitive to CP versus EP El Niño patterns. Focusing on the Atlantic, the Ohio basin's hydroclimate response shows substantial association with the WCW tripole SST pattern (Table S2 in Supporting Information S1). Thus, we suggest North Atlantic WCW tripole SSTA patterns exert a more dominant control on hydroclimate conditions over the Ohio basin compared to tropical Pacific forcing. Further analysis using instrumental observations consistently shows that WCW tripole SSTA patterns over the North Atlantic contribute to enhanced moisture supply, generating precipitation increases over the Ohio basin (Figure S14 and Text S2 in Supporting Information S1). In the SOM analyses of North Atlantic

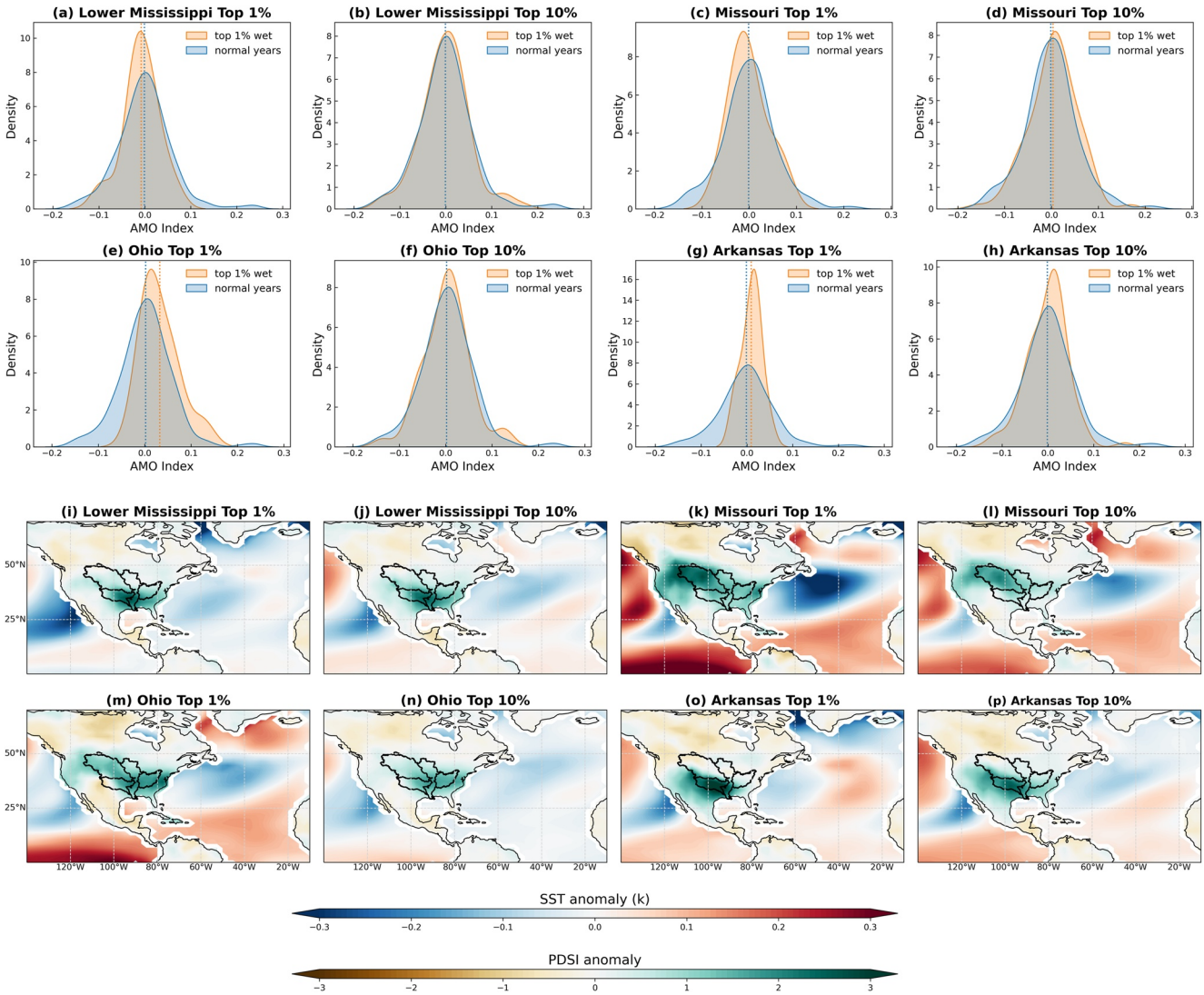

Figure 4. North Atlantic sea surface temperature impacts on hydroclimate conditions over the Mississippi River basin: (a–h) Show the probability density functions of the Atlantic Multi-Decadal Oscillation indices during wet extreme events (top 1% and 10%) over major tributaries (Lower Mississippi, Missouri, Ohio, and Arkansas), compared to those during normal years (IQR). The differences in the PDFs between wet extremes and normal years are only significant ($p < 0.05$ in Wilcoxon rank-sum test) for the top 1% wet conditions over the Ohio basin (e). Dotted lines represent the average of each distribution. (i–p) Show the sea surface temperature anomaly and Palmer Drought Severity Index anomaly composite maps during wet extreme events (top 1% and 10%) over the major tributaries. The Mississippi River basin and its major tributaries are outlined with black lines.

SSTs, the strong WCW pattern, which is significantly associated with wet conditions over the Missouri and Arkansas basins, is consistently connected to strong El Niño-like warming patterns over the tropical Pacific (Text S1 in Supporting Information S1). Instrumental observations show a slight precipitation increase over the Missouri and Arkansas basins for WCW tripole patterns (Figure S14 in Supporting Information S1). However, when compared to the influence of the tropical Pacific forcing pattern, the North Atlantic influence is muted in these regions (Text S2 in Supporting Information S1). This suggests that El Niño-like patterns over the tropical Pacific, rather than North Atlantic SST variability, exert a more dominant control on both Missouri and Arkansas basin hydroclimate over the LM.

4. Discussion and Conclusions

Developing adaptation strategies for a future with a dramatically altered hydrological cycle is an urgent global research priority for science and engineering (Alfieri et al., 2017; Kundzewicz et al., 2014). To this end, this

work seeks to improve our understanding of the dynamical causes of hydrologic extremes on the Mississippi River system. We used a state-of-the-art paleoclimate DA reconstruction spanning the LM (PHYDA) to provide a long-term contextualization for recent basin hydroclimate extremes. We diagnosed and partitioned the drivers of regional hydroclimate changes, focusing on the modes of natural variability known to alter modern hydrology in the basin: ENSO and North Atlantic SST variability. By assembling key metrics for climate variability and basin hydroclimate, we evaluated the controls on hydroclimate extremes throughout the Mississippi River basin over the LM.

We used SOM analyses to isolate the SST modes over the tropical Pacific that most frequently accompany extreme wet events over the Mississippi River basin and its major tributaries (Missouri, Ohio, Arkansas, and Lower Mississippi). We find that Mississippi River wet extremes are associated with strong El Niño-like warming. The Missouri and Arkansas basins dominate the forcing of wet extremes over the whole Mississippi River basin. We also differentiated El Niño events based on tropical Pacific SST patterns into CP and EP El Niño events to assess their impacts on hydroclimate changes. The entire Mississippi River basin experiences dry conditions during CP El Niño, but wetter conditions during EP El Niño, consistent with studies evaluating 20th century data (Liang et al., 2014; Ning & Bradley, 2015; Yu & Zou, 2013). These hydroclimate teleconnection differences are mainly associated with shifts in the position and strength of stationary wave trains triggered by CP and EP SST patterns (Guo et al., 2017; Patricola et al., 2020; Weng et al., 2007, 2009). Tributary basins show spatial heterogeneity in response to CP and EP El Niño events; in particular, the Ohio basin exhibits the largest difference between CP (dry) and EP (wet) El Niño events. Finally, in addition to ENSO, we investigated the North Atlantic SST patterns associated with Mississippi River wet extremes. Analyses of North Atlantic SST changes show that, WCW NAT SSTs (following the definition in Han et al. (2016)) exert a dominant impact on Ohio hydroclimate extremes, which are associated with westward moisture flow generated by the cyclonic circulation anomalies over the North Atlantic and subsequent moisture convergence over the Ohio basin (Figure S14 and Text S2 in Supporting Information S1).

These results harbor important implications for risk assessments under a changing climate, and can inform regional adaptation strategies in the long-term. Recent studies indicate predictive power out to 2-year lead times for ENSO events (X. Wu et al., 2021). The information from paleoclimate data generated here linking ENSO to Mississippi hydroclimate could be used for seasonal-to-interannual flood hazard prediction. In addition, large teleconnection nonstationarity may complicate decadal-scale prediction by compounding with anthropogenic influences on the climate variability and river channels/basins (Muñoz et al., 2018). As one example, Mississippi hydroclimate could be modified by increased CP El Niño frequency (Lee & McPhaden, 2010; Yeh et al., 2009) or strengthened ENSO teleconnections forced by anthropogenic warming (Fasullo et al., 2018). Future work must consider the ways in which atmospheric warming will be modulated by both ENSO and NAT/NASH over decadal timescales. Furthermore, by integrating atmospheric and hydrologic processes in observational and simulated datasets, future work could establish a framework to diagnose the role of internal variability on riverine flooding that could be applied to other large temperate river systems where similar uncertainties prevail. This work takes a first step toward formalizing these frameworks, using LM paleoclimate data to bolster our statistics surrounding ENSO and North Atlantic SST (AMO and NAT) impacts on seasonal hydroclimate extremes.

We acknowledge important limitations of this work. We rely on a single data assimilation product (PHYDA), which houses uncertainties. First, while PHYDA contains relatively robust proxy coverage from tree rings over the Mississippi Basin and coral records in the tropical Pacific, the reconstruction does lose variance back in time due to changes in proxy availability. The proxy coverage in both space and time relevant to our study contained in PHYDA is given in (Figure S1 in Supporting Information S1). Normalizing the data using a 30-year moving standard deviation, as described in the methods, may inflate the mean variance and the uncertainties back in the reconstruction, but avoids issues related to changing proxy availability. Second, paleoclimate DA relies on a climate model prior for spatial covariance information, and the CESM-LME prior for PHYDA contains biases. PHYDA's climate patterns are inherently tied to the spatial air-sea relationships in CESM, and larger ENSO variance in CESM compared to observations may amplify ENSO teleconnection patterns over the Mississippi river basin (Deser et al., 2012). However, PHYDA's SSTs are bias-corrected to more closely match observations (Steiger et al., 2019), which may partially remedy this problem. In addition, PHYDA, as a paleoclimate reconstruction, has fewer degrees of freedom than those seen in observations (Johnson, 2013). It is therefore more difficult to extract CP and EP patterns using a SOM analysis on PHYDA (Figure 2), but we were able to approximate the patterns using EOF analysis (Figure 3). It is possible that the EOF analysis is identifying patterns that are

not physically distinct in PHYDA. Nevertheless, the fact that the temporal evolution of PHYDA is proxy-driven bolsters our confidence in the primarily frequency-based analyses employed in this work (SOMs, PDFs, and composites). The choice of model prior employed in the DA has a necessarily large impact on SSTs and PDSI evaluated here (Amrhein et al., 2020; Parsons & Hakim, 2019); additional work is required to evaluate the sensitivity of the PHYDA reconstruction to other model priors (or observational priors). Finally, PHYDA is limited in its reconstruction of dynamically-informative variables such as geopotential height, sea level pressure, or winds. Skillful reconstructions of such variables are challenging given the available proxy data spanning the Common Era, however. Circulation and atmospheric dynamical information would shed light on the synoptic-scale patterns which transport moisture into the basin over time; with only SST and hydroclimate fields reconstructed at the surface, we are required to extrapolate how SST fields likely shift pressure surfaces, wind fields, and ultimately, moisture transport. To address this, we extrapolated dynamical information from instrumental reanalysis data to bolster our conclusions, and to evaluate the atmospheric circulation anomalies accompanying tropical Pacific and North Atlantic SST anomalies identified in PHYDA (Figures S12 and S13 in Supporting Information S1). Additional work evaluating these patterns in climate models and linking DA reconstruction patterns to model simulations would enhance these analyses, and such work is ongoing amongst the authors of this manuscript.

In closing, ensemble climate model simulations predict significant changes in hydroclimate extremes over the Mississippi River basin that harbor potential to catastrophically disrupt shipping, agriculture, fisheries, and industry in the central United States. The Mississippi and Gulf Coast regions are home to some of the busiest ports in the United States, and billions of dollars have been invested in flood mitigation and navigation infrastructure, with billions more proposed (Peyronnin et al., 2013). Much of this infrastructure is designed for the hydroclimatic conditions of the 20th century, but the hydroclimatology of the Mississippi River basin will likely change over the coming century (Tao et al., 2014; Van der Wiel et al., 2018). Recent floods have resulted in operational failures which shutdown barge traffic and interrupt Morganza spillway operations (Fahie, 2019). These events motivate the generation of robust constraints on the climate mechanisms controlling regional basin discharge events. Climate data spanning thousands of years at annual resolution can provide such constraints over long time scales. Understanding the climatic controls on flood hazard, specifically due to natural modes of variability like ENSO and the AMO, are required for risk assessments under a changing climate, and can inform regional adaptation strategies in the long-term. While actionable science may require longer extensions of this research, this work represents an important first step toward documenting the modes of natural variability that will compound with climate change to alter hydroclimate in the region. By analyzing data capturing past, present, and future climate and river discharge patterns for the Mississippi River basin, we hope to advance knowledge of future climate risks in the central and southeastern United States.

Conflict of Interest

The authors declare no conflicts of interest relevant to this study.

Data Availability Statement

All of the DA product datasets used in this analysis are publicly available:

- PHYDA (https://doi.org/10.5281/zenodo.1198817).
- Global PDSI (https://wbwaterdata.org/dataset/global-pdsi, Sheffield et al., 2006, 2012) and (https://downloads.psl.noaa.gov/Datasets/dai_pdsi/, Dai et al., 2004).
- NOAA Extended Reconstructed SST V5 (ERSSTv5) (https://psl.noaa.gov/data/gridded/data.noaa.ersst.v5.html, Huang et al., 2017).
- NCEP-NCAR Reanalysis 1 (https://psl.noaa.gov/data/gridded/data.ncep.reanalysis.html, Kalnay et al., 1996).
- Global Precipitation Climatology Center (GPCC) (https://opendata.dwd.de/climate_environment/GPCC/html/fulldata-monthly_v2022_doi_download.html, Markus et al., 2022).

Acknowledgments
This work was supported by the National Oceanic and Atmospheric Administration (NOAA Award Number NA18OAR4310427) awarded to S.D., the National Science Foundation (NSF CLD-214778) to S.D. and S.M., and by a graduate fellowship from the Department of Earth, Environmental, and Planetary Sciences at Rice University to X.L. N.S. was supported in part by NSF AGS-1805490 and ISF 2654/20.

References

Alfieri, L., Bisselink, B., Dottori, F., Naumann, G., de Roo, A., Salamon, P., et al. (2017). Global projections of river flood risk in a warmer world. *Earth's Future*, *5*(2), 171–182. https://doi.org/10.1002/2016ef000485

Alfortish, M., Brandon, T., Gilbert, R., Stark, T., & Westerink, J. (2012). Geotechnical reconnaissance of the 2011 flood on the lower Mississippi River. In *Geo-engineering extreme event response report*. National Science Foundation.

Allison, M. A., Demas, C. R., Ebersole, B. A., Kleiss, B. A., Little, C. D., Meselhe, E. A., et al. (2012). A water and sediment budget for the lower Mississippi–Atchafalaya River in flood years 2008–2010: Implications for sediment discharge to the oceans and coastal restoration in Louisiana. *Journal of Hydrology*, *432*, 84–97. https://doi.org/10.1016/j.jhydrol.2012.02.020

Amrhein, D. E., Hakim, G. J., & Parsons, L. A. (2020). Quantifying structural uncertainty in paleoclimate data assimilation with an application to the last millennium. *Geophysical Research Letters*, *47*(22), e2020GL090485. https://doi.org/10.1029/2020gl090485

Ashok, K., Behera, S. K., Rao, S. A., Weng, H., & Yamagata, T. (2007). El Niño Modoki and its possible teleconnection. *Journal of Geophysical Research*, *112*(C11), C11007. https://doi.org/10.1029/2006jc003798

Barry, J. M. (2007). *Rising tide: The great Mississippi flood of 1927 and how it changed America*. Simon and Schuster.

Cayan, D. R. (1980). Large-scale relationships between sea surface temperature and surface air temperature. *Monthly Weather Review*, *108*(9), 1293–1301. https://doi.org/10.1175/1520-0493(1980)108<1293:lsrbss>2.0.co;2

Chen, J., & Kumar, P. (2002). Role of terrestrial hydrologic memory in modulating ENSO impacts in North America. *Journal of Climate*, *15*(24), 3569–3585. https://doi.org/10.1175/1520-0442(2003)015<3569:rothmi>2.0.co;2

Chen, S., Wu, R., & Chen, W. (2020). Strengthened connection between springtime North Atlantic oscillation and North Atlantic tripole SST pattern since the late 1980s. *Journal of Climate*, *33*(5), 2007–2022. https://doi.org/10.1175/jcli-d-19-0628.1

Dai, A., Qian, T., Trenberth, K. E., & Milliman, J. D. (2009). Changes in continental freshwater discharge from 1948 to 2004. *Journal of Climate*, *22*(10), 2773–2792. https://doi.org/10.1175/2008jcli2592.1

Dai, A., Trenberth, K. E., & Qian, T. (2004). A global dataset of Palmer Drought Severity Index for 1870–2002: Relationship with soil moisture and effects of surface warming. *Journal of Hydrometeorology*, *5*(6), 1117–1130. https://doi.org/10.1175/jhm-386.1

Dee, S., Okumura, Y., Stevenson, S., & Di Nezio, P. (2020). Enhanced North American ENSO teleconnections during the Little Ice Age revealed by paleoclimate data assimilation. *Geophysical Research Letters*, *47*(15), e2020GL087504. https://doi.org/10.1029/2020gl087504

Dee, S. G., & Steiger, N. J. (2022). ENSO's response to volcanism in a data assimilation-based paleoclimate reconstruction over the Common Era. *Paleoceanography and Paleoclimatology*, *37*(3), e2021PA004290. https://doi.org/10.1029/2021pa004290

Deser, C., Phillips, A. S., Tomas, R. A., Okumura, Y. M., Alexander, M. A., Capotondi, A., et al. (2012). ENSO and Pacific decadal variability in the community climate system model version 4. *Journal of Climate*, *25*(8), 2622–2651. https://doi.org/10.1175/jcli-d-11-00301.1

Durkee, J., Frye, J., Fuhrmann, C., Lacke, M., Jeong, H., & Mote, T. (2008). Effects of the North Atlantic Oscillation on precipitation-type frequency and distribution in the eastern United States. *Theoretical and Applied Climatology*, *94*(1), 51–65. https://doi.org/10.1007/s00704-007-0345-x

Enfield, D. B., Mestas-Nuñez, A. M., & Trimble, P. J. (2001). The Atlantic multidecadal oscillation and its relation to rainfall and river flows in the continental US. *Geophysical Research Letters*, *28*(10), 2077–2080. https://doi.org/10.1029/2000gl012745

Fahie, M. (2019). *Impacts of the 2019 Upper Mississippi River flooding on barge movements in the Upper Midwest Region*. USCG Sector Upper Mississippi River.

Fasullo, J., Otto-Bliesner, B., & Stevenson, S. (2018). ENSO's changing influence on temperature, precipitation, and wildfire in a warming climate. *Geophysical Research Letters*, *45*(17), 9216–9225. https://doi.org/10.1029/2018gl079022

Feng, S., Hu, Q., & Oglesby, R. J. (2011). Influence of Atlantic sea surface temperatures on persistent drought in North America. *Climate Dynamics*, *37*(3), 569–586. https://doi.org/10.1007/s00382-010-0835-x

Guo, Y., Ting, M., Wen, Z., & Lee, D. E. (2017). Distinct patterns of tropical Pacific SST anomaly and their impacts on North American climate. *Journal of Climate*, *30*(14), 5221–5241. https://doi.org/10.1175/jcli-d-16-0488.1

Hakim, G. J., Emile-Geay, J., Steig, E. J., Noone, D., Anderson, D. M., Tardif, R., et al. (2016). The last millennium climate reanalysis project: Framework and first results. *Journal of Geophysical Research: Atmospheres*, *121*(12), 6745–6764. https://doi.org/10.1002/2016jd024751

Han, Z., Luo, F., & Wan, J. (2016). The observational influence of the North Atlantic SST tripole on the early spring atmospheric circulation. *Geophysical Research Letters*, *43*(6), 2998–3003. https://doi.org/10.1002/2016gl068099

Horton, D. E., Johnson, N. C., Singh, D., Swain, D. L., Rajaratnam, B., & Diffenbaugh, N. S. (2015). Contribution of changes in atmospheric circulation patterns to extreme temperature trends. *Nature*, *522*(7557), 465–469. https://doi.org/10.1038/nature14550

Hu, Q., Feng, S., & Oglesby, R. J. (2011). Variations in North American summer precipitation driven by the Atlantic multidecadal oscillation. *Journal of Climate*, *24*(21), 5555–5570. https://doi.org/10.1175/2011jcli4060.1

Huang, B., Thorne, P. W., Banzon, V. F., Boyer, T., Chepurin, G., Lawrimore, J. H., et al. (2017). *NOAA extended reconstructed sea surface temperature (ERSST), version 5* (Vol. 30, pp. 8179–8205). NOAA National Centers for Environmental Information.

Johnson, N. C. (2013). How many ENSO flavors can we distinguish? *Journal of Climate*, *26*(13), 4816–4827. https://doi.org/10.1175/jcli-d-12-00649.1

Johnson, N. C., Feldstein, S. B., & Tremblay, B. (2008). The continuum of Northern Hemisphere teleconnection patterns and a description of the NAO shift with the use of self-organizing maps. *Journal of Climate*, *21*(23), 6354–6371. https://doi.org/10.1175/2008jcli2380.1

Kalnay, E., Kanamitsu, M., Kistler, R., Collins, W., Deaven, D., Gandin, L., et al. (1996). The NCEP/NCAR 40-year reanalysis project. *Bulletin of the American Meteorological Society*, *77*(3), 437–472. https://doi.org/10.1175/1520-0477(1996)077<0437:tnyrp>2.0.co;2

Kao, H.-Y., & Yu, J.-Y. (2009). Contrasting eastern-Pacific and central-Pacific types of ENSO. *Journal of Climate*, *22*(3), 615–632. https://doi.org/10.1175/2008jcli2309.1

Kiem, A. S., Franks, S. W., & Kuczera, G. (2003). Multi-decadal variability of flood risk. *Geophysical Research Letters*, *30*(2), 1035. https://doi.org/10.1029/2002gl015992

Kohonen, T. (1990). The self-organizing map. *Proceedings of the IEEE*, *78*(9), 1464–1480. https://doi.org/10.1109/5.58325

Kug, J.-S., Jin, F.-F., & An, S.-I. (2009). Two types of El Niño events: Cold tongue El Niño and warm pool El Niño. *Journal of Climate*, *22*(6), 1499–1515. https://doi.org/10.1175/2008jcli2624.1

Kundzewicz, Z. W., Kanae, S., Seneviratne, S. I., Handmer, J., Nicholls, N., Peduzzi, P., et al. (2014). Flood risk and climate change: Global and regional perspectives. *Hydrological Sciences Journal*, *59*(1), 1–28. https://doi.org/10.1080/02626667.2013.857411

Lee, T., & McPhaden, M. J. (2010). Increasing intensity of El Niño in the central-equatorial Pacific. *Geophysical Research Letters*, *37*(14), L14603. https://doi.org/10.1029/2010gl044007

Liang, Y.-C., Lo, M.-H., & Yu, J.-Y. (2014). Asymmetric responses of land hydroclimatology to two types of El Niño in the Mississippi River Basin. *Geophysical Research Letters*, *41*(2), 582–588. https://doi.org/10.1002/2013gl058828

Liu, Y., & Weisberg, R. H. (2011). A review of self-organizing map applications in meteorology and oceanography. In *Self-Organizing Maps: Applications and Novel Algorithm Design* (Vol. *1*, pp. 253–272).
Liu, Y., Weisberg, R. H., & Mooers, C. N. (2006). Performance evaluation of the self-organizing map for feature extraction. *Journal of Geophysical Research*, *111*(C5), C05018. https://doi.org/10.1029/2005jc003117
Luo, X., Dee, S., Stevenson, S., Okumura, Y., Steiger, N., & Parsons, L. (2022). Last millennium ENSO diversity and North American teleconnections: New insights from paleoclimate data assimilation. *Paleoceanography and Paleoclimatology*, *37*(3), e2021PA004283. https://doi.org/10.1029/2021pa004283
Mallakpour, I., & Villarini, G. (2016). Investigating the relationship between the frequency of flooding over the central United States and large-scale climate. *Advances in Water Resources*, *92*, 159–171. https://doi.org/10.1016/j.advwatres.2016.04.008
Markus, Z., Rauthe-Schöch, A., Hänsel, S., Finger, P., Rustemeier, E., & Schneider, U. (2022). *GPCC full data daily version 2022 at 1.0°: Daily land-surface precipitation from rain-gauges built on GTS-based and historic data*. Global Precipitation Climatology Centre (GPCC) at Deutscher Wetterdienst. https://doi.org/10.5676/DWD_GPCC/FD_D_V2022_100
McCabe, G. J., & Wolock, D. M. (2014). Spatial and temporal patterns in conterminous United States streamflow characteristics. *Geophysical Research Letters*, *41*(19), 6889–6897. https://doi.org/10.1002/2014gl061980
Muñoz, S. E., & Dee, S. G. (2017). El Niño increases the risk of lower Mississippi River flooding. *Scientific Reports*, *7*(1), 1–7. https://doi.org/10.1038/s41598-017-01919-6
Muñoz, S. E., Giosan, L., Therrell, M. D., Remo, J. W., Shen, Z., Sullivan, R. M., et al. (2018). Climatic control of Mississippi River flood hazard amplified by river engineering. *Nature*, *556*(7699), 95–98. https://doi.org/10.1038/nature26145
Ning, L., & Bradley, R. S. (2015). Influence of eastern Pacific and central Pacific El Niño events on winter climate extremes over the eastern and central United States. *International Journal of Climatology*, *35*(15), 4756–4770. https://doi.org/10.1002/joc.4321
Oke, P. R., Allen, J. S., Miller, R. N., Egbert, G. D., & Kosro, P. M. (2002). Assimilation of surface velocity data into a primitive equation coastal ocean model. *Journal of Geophysical Research*, *107*(C9), 5–1. https://doi.org/10.1029/2000jc000511
Otto-Bliesner, B. L., Brady, E. C., Fasullo, J., Jahn, A., Landrum, L., Stevenson, S., et al. (2016). Climate variability and change since 850 CE: An ensemble approach with the Community Earth System Model. *Bulletin of the American Meteorological Society*, *97*(5), 735–754. https://doi.org/10.1175/bams-d-14-00233.1
PAGES2k Consortium. (2017). A global multiproxy database for temperature reconstructions of the Common Era. *Scientific Data*, *4*(1), 170088. https://doi.org/10.1038/sdata.2017.88
Palmer, W. C. (1965). *Meteorological drought* (Vol. 30). US Department of Commerce, Weather Bureau.
Parsons, L., & Hakim, G. (2019). Local regions associated with interdecadal global temperature variability in the last millennium reanalysis and CMIP5 models. *Journal of Geophysical Research: Atmospheres*, *124*(17–18), 9905–9917. https://doi.org/10.1029/2019jd030426
Patricola, C. M., O'Brien, J. P., Risser, M. D., Rhoades, A. M., O'Brien, T. A., Ullrich, P. A., et al. (2020). Maximizing ENSO as a source of western US hydroclimate predictability. *Climate Dynamics*, *54*(1–2), 351–372. https://doi.org/10.1007/s00382-019-05004-8
Peng, S., Robinson, W. A., & Li, S. (2003). Mechanisms for the NAO responses to the North Atlantic SST tripole. *Journal of Climate*, *16*(12), 1987–2004. https://doi.org/10.1175/1520-0442(2003)016<1987:mftnrt>2.0.co;2
Peyronnin, N., Green, M., Richards, C. P., Owens, A., Reed, D., Chamberlain, J., et al. (2013). Louisiana's 2012 Coastal Master Plan: Overview of a science-based and publicly informed decision-making process. *Journal of Coastal Research*, *67*(10067), 1–15. https://doi.org/10.2112/si_67_1.1
Rogers, J. C., & Coleman, J. S. (2003). Interactions between the Atlantic multidecadal oscillation, El Nino/La Nina, and the PNA in winter Mississippi valley stream flow. *Geophysical Research Letters*, *30*(10), 1518. https://doi.org/10.1029/2003gl017216
Sheffield, J., Goteti, G., & Wood, E. F. (2006). Development of a 50-year high-resolution global dataset of meteorological forcings for land surface modeling. *Journal of Climate*, *19*(13), 3088–3111. https://doi.org/10.1175/jcli3790.1
Sheffield, J., Wood, E. F., & Roderick, M. L. (2012). Little change in global drought over the past 60 years. *Nature*, *491*(7424), 435–438. https://doi.org/10.1038/nature11575
Smith, J. A., & Baeck, M. L. (2015). "Prophetic vision, vivid imagination": The 1927 Mississippi River flood. *Water Resources Research*, *51*(12), 9964–9994. https://doi.org/10.1002/2015wr017927
Smith, L. M., & Winkley, B. R. (1996). The response of the Lower Mississippi River to river engineering. *Engineering Geology*, *45*(1–4), 433–455. https://doi.org/10.1016/s0013-7952(96)00025-7
Stedinger, J. R., & Griffis, V. W. (2011). Getting from here to where? Flood frequency analysis and climate 1. *JAWRA Journal of the American Water Resources Association*, *47*(3), 506–513. https://doi.org/10.1111/j.1752-1688.2011.00545.x
Steiger, N. J., Smerdon, J. E., Cook, B. I., Seager, R., Williams, A. P., & Cook, E. R. (2019). Oceanic and radiative forcing of medieval megadroughts in the American Southwest. *Science Advances*, *5*(7), eaax0087. https://doi.org/10.1126/sciadv.aax0087
Steiger, N. J., Smerdon, J. E., Cook, E. R., & Cook, B. I. (2018). A reconstruction of global hydroclimate and dynamical variables over the Common Era. *Scientific Data*, *5*(1), 1–15. https://doi.org/10.1038/sdata.2018.86
Stevenson, S. (2012). Significant changes to ENSO strength and impacts in the twenty-first century: Results from CMIP5. *Geophysical Research Letters*, *39*(17), 17703. https://doi.org/10.1029/2012gl052759
Sutton, R. T., Norton, W. A., & Jewson, S. P. (2000). The North Atlantic oscillation—What role for the ocean? *Atmospheric Science Letters*, *1*(2), 89–100. https://doi.org/10.1006/asle.2000.0018
Takahashi, K., Montecinos, A., Goubanova, K., & Dewitte, B. (2011). ENSO regimes: Reinterpreting the canonical and Modoki El Niño. *Geophysical Research Letters*, *38*(10), L10707. https://doi.org/10.1029/2011gl047364
Tao, B., Tian, H., Ren, W., Yang, J., Yang, Q., He, R., et al. (2014). Increasing Mississippi river discharge throughout the 21st century influenced by changes in climate, land use, and atmospheric CO_2. *Geophysical Research Letters*, *41*(14), 4978–4986. https://doi.org/10.1002/2014gl060361
Tardif, R., Hakim, G. J., Perkins, W. A., Horlick, K. A., Erb, M. P., Emile-Geay, J., et al. (2019). Last Millennium Reanalysis with an expanded proxy database and seasonal proxy modeling. *Climate of the Past*, *15*(4), 1251–1273. https://doi.org/10.5194/cp-15-1251-2019
Tootle, G. A., Piechota, T. C., & Singh, A. (2005). Coupled oceanic-atmospheric variability and US streamflow. *Water Resources Research*, *41*(12), 12408. https://doi.org/10.1029/2005wr004381
Twine, T. E., Kucharik, C. J., & Foley, J. A. (2005). Effects of El Niño–Southern oscillation on the climate, water balance, and streamflow of the Mississippi River basin. *Journal of Climate*, *18*(22), 4840–4861. https://doi.org/10.1175/jcli3566.1
Van der Wiel, K., Kapnick, S. B., Vecchi, G. A., Smith, J. A., Milly, P. C., & Jia, L. (2018). 100-year lower Mississippi floods in a global climate model: Characteristics and future changes. *Journal of Hydrometeorology*, *19*(10), 1547–1563. https://doi.org/10.1175/jhm-d-18-0018.1
Weng, H., Ashok, K., Behera, S. K., Rao, S. A., & Yamagata, T. (2007). Impacts of recent El Niño Modoki on dry/wet conditions in the Pacific rim during boreal summer. *Climate Dynamics*, *29*(2–3), 113–129. https://doi.org/10.1007/s00382-007-0234-0

Weng, H., Behera, S. K., & Yamagata, T. (2009). Anomalous winter climate conditions in the Pacific rim during recent El Niño Modoki and El Niño events. *Climate Dynamics*, *32*(5), 663–674. https://doi.org/10.1007/s00382-008-0394-6

Wu, X., Okumura, Y. M., Deser, C., & DiNezio, P. N. (2021). Two-year dynamical predictions of ENSO event duration during 1954–2015. *Journal of Climate*, *34*(10), 4069–4087. https://doi.org/10.1175/jcli-d-20-0619.1

Wu, Z., Wang, B., Li, J., & Jin, F.-F. (2009). An empirical seasonal prediction model of the East Asian summer monsoon using ENSO and NAO. *Journal of Geophysical Research*, *114*(D18), D18120. https://doi.org/10.1029/2009jd011733

Yeh, S.-W., Kug, J.-S., Dewitte, B., Kwon, M.-H., Kirtman, B. P., & Jin, F.-F. (2009). El Niño in a changing climate. *Nature*, *461*(7263), 511–514. https://doi.org/10.1038/nature08316

Yu, J.-Y., & Zou, Y. (2013). The enhanced drying effect of Central-Pacific El Niño on US winter. *Environmental Research Letters*, *8*(1), 014019. https://doi.org/10.1088/1748-9326/8/1/014019